Plasma Sources Science and Technology

PAPER • OPEN ACCESS

Impact of the electrode proximity on the streamer breakdown and development of pulsed dielectric barrier discharges

To cite this article: J R Wubs *et al* 2022 *Plasma Sources Sci. Technol.* **31** 035006

View the article online for updates and enhancements.

You may also like

- Streamer inception thresholds derived from a statistical electron transport model
Raphael Färber and Christian M. Franck
- The diameters of long positive streamers in atmospheric air under lightning impulse voltage
She Chen, Rong Zeng and Chijie Zhuang
- Streamer breakdown: cathode spot formation, Trichel pulses and cathode-sheath instabilities
Mirko ernák, Tomáš Hoder and Zdenk Bonaventura

This content was downloaded from IP address 89.245.22.200 on 06/03/2023 at 07:43

OPEN ACCESS
IOP Publishing
Plasma Sources Science and Technology
Plasma Sources Sci. Technol. **31** (2022) 035006 (10pp)
https://doi.org/10.1088/1361-6595/ac511f

Impact of the electrode proximity on the streamer breakdown and development of pulsed dielectric barrier discharges

J R Wubs[1,2,*], H Höft[1], M Kettlitz[1], M M Becker[1] and K-D Weltmann[1]

[1] Leibniz Institute for Plasma Science and Technology (INP Greifswald), Felix-Hausdorff-Str. 2, 17489 Greifswald, Germany
[2] Eindhoven University of Technology, PO Box 513, 5600 MB Eindhoven, The Netherlands

E-mail: jente.wubs@inp-greifswald.de and hans.hoeft@inp-greifswald.de

Received 19 November 2021, revised 20 January 2022
Accepted for publication 2 February 2022
Published 8 March 2022

Abstract

The impact of the electrode proximity on the streamer breakdown and development of pulsed-driven dielectric barrier discharges (DBDs) in a single-filament arrangement has been investigated in a gas mixture of 0.1 vol% O_2 in N_2 at 0.6 bar and 1.0 bar. The gap distance was varied from 0.5 mm to 1.5 mm, and the applied voltage was adapted correspondingly to create comparable breakdown conditions in the gap. The development of the DBDs was recorded by an iCCD and a streak camera system, while fast electrical measurements provided insight into discharge characteristics such as the transferred charge and consumed energy. The results demonstrate that breakdown in a smaller gap is characterised by a slower streamer propagation but a significantly higher acceleration. It can therefore be concluded that the proximity of the cathode has a strong impact on the characteristics of the streamer breakdown. However, after the streamer has crossed the gap, the discharge structure in front of the anode was found to be the same independent of the actual gap distance.

Keywords: dielectric barrier discharge, streamer, electrical and optical diagnostics

(Some figures may appear in colour only in the online journal)

1. Introduction

Atmospheric pressure discharges that generate non-thermal plasmas are of particular interest for a wide variety of applications, including pollution control [1], plasma medicine [2] and more recently plasma agriculture [3]. In these 'cold' plasmas only the electrons feature high energies, while the heavy particles stay near room temperature. Therefore, such plasmas are used in many industrial applications to enable an energy-efficient and effective plasma chemistry for the production of reactive species [4–6]. A common tool for the generation of these plasmas is the dielectric barrier discharge (DBD) [7]. This type of discharge is characterised by the presence of at least one insulator in the discharge gap between the electrodes [7]. This so-called dielectric barrier limits the electrical current and thus avoids thermalisation (i.e. a transition to a spark or arc discharge), leading to the generation of a non-thermal plasma [4, 8].

Generally, DBDs in a gas gap at elevated pressures in air-like gas mixtures consist of constricted volume discharge channels, often referred to as filaments, and surface discharge channels spreading on the dielectric barrier(s) [9, 10]. Apart from volume discharges in the gap between electrodes, there are plasma devices where discharges ignite inside confined environments such as μm-sized cavities [11] or capillary channels [12]. Furthermore, there are surface DBDs that feature no gas gap, i.e. the electrodes are directly mounted on or embedded in the dielectric [13–15].

* Author to whom any correspondence should be addressed.

Original content from this work may be used under the terms of the Creative Commons Attribution 4.0 licence. Any further distribution of this work must maintain attribution to the author(s) and the title of the work, journal citation and DOI.

 © 2022 The Author(s). Published by IOP Publishing Ltd

The gap distances used for volume DBDs are in most cases in the (sub-)mm range [16]. Consequently, the volume-to-surface ratio is varying significantly depending on the electrode configuration and the gap distance, i.e. especially for short gaps the surface will have a significant impact. The importance of the dielectric surface on the discharge development is manifold. First of all, charge deposition on dielectric barriers is crucial for the principle of DBDs, as the accumulation of surface charges weakens the applied electric field in the gap, leading to a transient discharge behaviour that is characteristic for DBDs [15]. Additionally, in a common plate-to-plate DBD arrangement, localised surface charge spots deposited during the preceding discharge event determine the position of subsequent filaments, known as the surface memory effect [17, 18]. Residual surface charges have however also been reported to be responsible for the temporal jitter of the discharge inception rather than memorising the filament position [19]. Next to this, the accumulation of surface charges modifies the electric field distribution in the discharge gap, that affects the accumulation of positive space charges in front of the anode, i.e. the pre-breakdown phase prior to the propagation of a cathode-directed ionisation front (positive streamer) [19, 20]. Lastly, the streamer development in the gap is influenced by the modified electric field as well, that is especially of importance when the streamer reaches the proximity of the dielectric surface [21].

Although there are some works (e.g. [22, 23]) that report on the impact of the gap distance on electrical characteristics, detailed studies on the impact of the electrode proximity on the breakdown and development of DBDs are still missing. However, experimental investigations on this are essential as a basis for the validation of models that are necessary to gain a comprehensive overview of the discharge behaviour [24–27].

For fundamental investigations of the DBD breakdown and development, a so-called single-filament arrangement is often used, where the spatial filament stabilisation is achieved by using two hemispherical-shaped pin electrodes covered by a dielectric [28]. Additionally, pulsed-operation of DBDs in this specific configuration provides temporal stability of the discharge inception and reproducible individual discharge events [29, 30].

A similar double-sided arrangement with a variable gap distance was used for the present work, since the aim of this study is investigating how the proximity of the dielectric-covered electrodes impacts the breakdown and development of volume DBDs. To enable conditions that allow a comparison between different gap distances and pressures, the applied voltage had to be adapted for each gap distance (0.5 mm, 1.0 mm, and 1.5 mm) and pressure (0.6 bar and 1.0 bar). The results presented in this paper include a full electrical characterisation of essential quantities such as the transferred charge and consumed electrical energy. Furthermore, a comparison of the overall discharge structure and diameter was performed for different gap distances and pressures, as well as an accurate tracing of the streamer propagation that reveals how the streamer development is influenced by the proximity of the electrode surface.

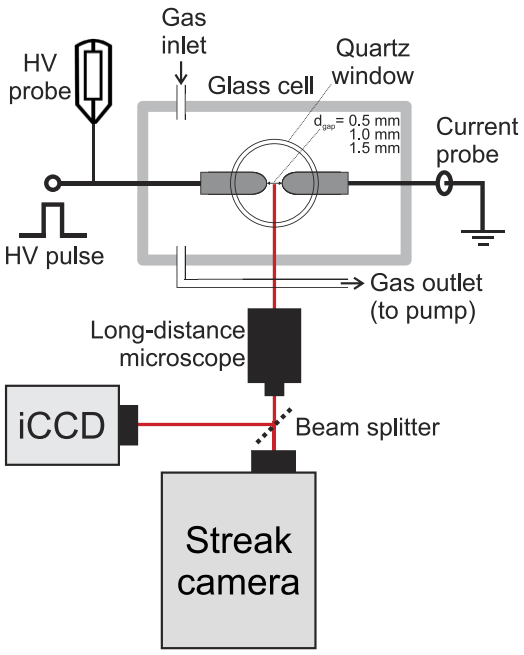

Figure 1. Schematic overview of the discharge arrangement and the applied optical and electrical diagnostics.

2. Experimental arrangement and diagnostics

A symmetric double-sided arrangement with hemispherical alumina (Al_2O_3) covered metal electrodes was used for investigating single-filament DBDs. The thickness of the dielectric barriers was (0.50 ± 0.05) mm and the radius of curvature of their surface was (2.0 ± 0.1) mm. The gap distance between the electrodes was set to 0.5 mm, 1.0 mm or 1.5 mm, respectively, with a maximum error of 3%. The electrodes were implemented in a gas cell made of glass with two lateral quartz glass windows that allowed the observation of the DBDs from the UV to the near-infrared. The cell had a gas inlet at the top and an outlet to a vacuum pumping system at the bottom, as illustrated in figure 1. Before filling the cell with a specific gas mixture, it was evacuated to $p < 10^{-4}$ mbar by a turbopump system (Pfeiffer, TSH261), and subsequently an additional membrane pump (Pfeiffer, MVP 020-3 AC) was used as a process pump in a bypass to adjust the pressure in the cell to either 0.6 bar or 1.0 bar. The gas flow through the cell was set to 100 sccm by mass flow controllers (MKS 179B with control unit MKS 647B) connected to gas cylinders (Air Liquide, gas purity 99.999%). A gas mixture of 0.1 vol% O_2 in N_2 was used for all experiments.

The DBDs were driven by unipolar positive square wave pulses with a repetition rate of 10 kHz and a pulse width of 1 μs (and equivalently a pause time t_{pause} of 99 μs). To create similar breakdown conditions in the gap that allow a comparison between different gap distances and pressures, each change in the gap distance or pressure had to be accompanied by a change in the applied voltage. The amplitude of the applied voltage pulses was therefore systematically varied between 4 and 14 kV, with the minimum and maximum values depending on the gap distance and pressure. Based on this voltage

variation, a suitable voltage amplitude was selected for each pressure and gap distance; the selection criteria used for this are discussed in more detail further on in the text. The shape of the voltage pulses was specified by the high voltage pulse generator (Behlke, HTS 161 − 06 GSM) that was supplied by a high-voltage power supply (FUG, HCN 1400-12500) and controlled by a digital delay generator (NI, DG645).

Electrical measurements were performed with fast voltage (Tektronix, P6015A) and current probes (custom-build according to [31]) and recorded with a digital sampling oscilloscope (R & S, RTO 1044, 4 GHz, 20 GS/s). The DBDs were observed simultaneously by an iCCD camera (Andor, iStar DH734-18U-A3) and a streak camera system (Hamamatsu, C5680-21C) connected to a long-distance microscope (Questar, QM100, UV transparent), as shown in figure 1. The iCCD camera enabled the recording of two-dimensional images of single DBDs and their propagation on the electrode surfaces (resolution: $\Delta t \geqslant 2$ ns, $\Delta x \geqslant 2$ μm), while the streak images yielded the spatio-temporal DBD development along the central axis of the discharge channel, with high temporal ($\Delta t \geqslant 20$ ps) and spatial ($\Delta x \geqslant 2$ μm) resolutions. Imaging the complete discharge in a 1.5 mm gap required a reduction of the magnification produced by the long-distance microscope by a factor of approximately 1.5, leading to a lower spatial resolution in this case. Both cameras were sensitive in the UV and visible spectral range, and all images presented in this paper were recorded spectrally-integrated.

3. Results and discussion

First, an electrical characterisation of the investigated discharges is given, based on which specific cases have been selected for the comparison of different gap distances and pressures. The results of the electrical measurements for a 1.5 mm discharge gap and a pressure of 1.0 bar are presented in figure 2. Here, figure 2(a) exemplarily displays the voltage and current development for a complete pulse of 10 kV. The pulsed operation leads to one single DBD at the rising slope and one at the falling slope. This paper only focuses on DBDs at the rising slope to minimise additional effects of the preceding DBD on the investigated discharge characteristics. The temporal jitter of the discharges at the rising slope is $\leqslant$1 ns. Hence, averaging hardly affects the shape of the current peak and the measurements were averaged over 1000 individual discharge events to obtain the presented results.

Figure 2(b) shows the detailed structure of the applied voltage V and corresponding current at the rising slope in a 250-ns time window. The measured current I_{tot} consists of the displacement current I_{disp} and the discharge current I_{DBD}. To determine I_{DBD}, the displacement current was measured for all investigated cases and for all different pulse amplitudes with the corresponding voltage waveform applied, but without immediate ignition of the discharge. With this, the discharge current flowing through the gap was calculated according to the relation given in [32]:

$$I_{\mathrm{DBD}} = \frac{C_{\mathrm{b}}/2}{C_{\mathrm{b}}/2 - C_{\mathrm{tot}}} \left(I_{\mathrm{tot}} - I_{\mathrm{disp}}\right). \tag{1}$$

Here, $C_{\mathrm{b}}/2$ is the combined capacitance of the two dielectric barriers and C_{tot} the total capacitance of the DBD arrangement, that can both be extracted from a Q–V plot, as shown in figure 2(d).

The resulting discharge current is presented in figure 2(c) for three different pulse amplitudes. The rise time (10% to 90%) of the applied voltage was specified by the pulse generator and it was approximately 60 ns regardless of the pulse amplitude. Varying the pulse amplitude therefore led to a different voltage slope steepness and a corresponding shift in the discharge inception time, as can be seen in figure 2(c). It has been reported in a previous work that a steeper voltage slope in general leads to higher breakdown voltages, larger electrical currents and an increased amount of charges transferred within single discharge events [33]. These effects are in this study overlapping with the consequences of increasing the voltage amplitude, which has a similar impact on the discharge characteristics [34]. In other words, increasing the voltage amplitude and increasing the voltage slope steepness both contribute to the aforementioned effects. The increased amount of charges created in the case of a higher voltage amplitude and steeper slope results in an elevated pre-ionisation level, i.e. a higher amount of charges still present in the gap after $t_{\mathrm{pause}} = 99$ μs. Pre-ionisation is known to be responsible for the generation of stable discharges, but above a certain threshold it can also significantly affect the discharge development, which is manifested by e.g. a reduction of the breakdown voltage and a decrease in the current maximum [30]. This can be clearly observed in figure 2(c) for the case of $V_{\mathrm{pulse}} = 14$ kV. However, such pre-ionisation effects are undesirable in this study, for which the focus is on effects related to the proximity of the electrode surfaces. Lowering the repetition rate would be a straightforward way to reduce the pre-ionisation level, but this leads in some cases to the generation of discharges that are either temporally or spatially unstable. For this reason, a repetition rate of 10 kHz was chosen in this study. For the comparison between different gap distances only cases were considered for which effects due to an elevated pre-ionisation level can be neglected.

The time integration of the total current provides the time development of the charge $Q(t)$. In combination with the applied voltage $V(t)$ this allows drawing a Q–V plot that reveals discharge characteristics such as the consumed electrical energy E_{el} and the capacitances of the DBD arrangement. In doing so, it is important to synchronise the measured voltage and current signals based on the relation between the time derivative of the voltage, the displacement current and the total capacitance of the DBD arrangement [32]:

$$I_{\mathrm{disp}}(t) = C_{\mathrm{tot}} \frac{\mathrm{d}V(t)}{\mathrm{d}t}. \tag{2}$$

The obtained Q–V plots for $d_{\mathrm{gap}} = 1.5$ mm and $p = 1.0$ bar are given in figure 2(d). The slope during the off-phase of the discharge (see figure 2(d)) provides the total capacitance $C_{\mathrm{tot}} = (0.28 \pm 0.01)$ pF. Additionally, the combined capacitance of the two dielectric barriers can be calculated from the slope of a fitting line through the upper right corners of Q–V plots for different voltage pulse amplitudes

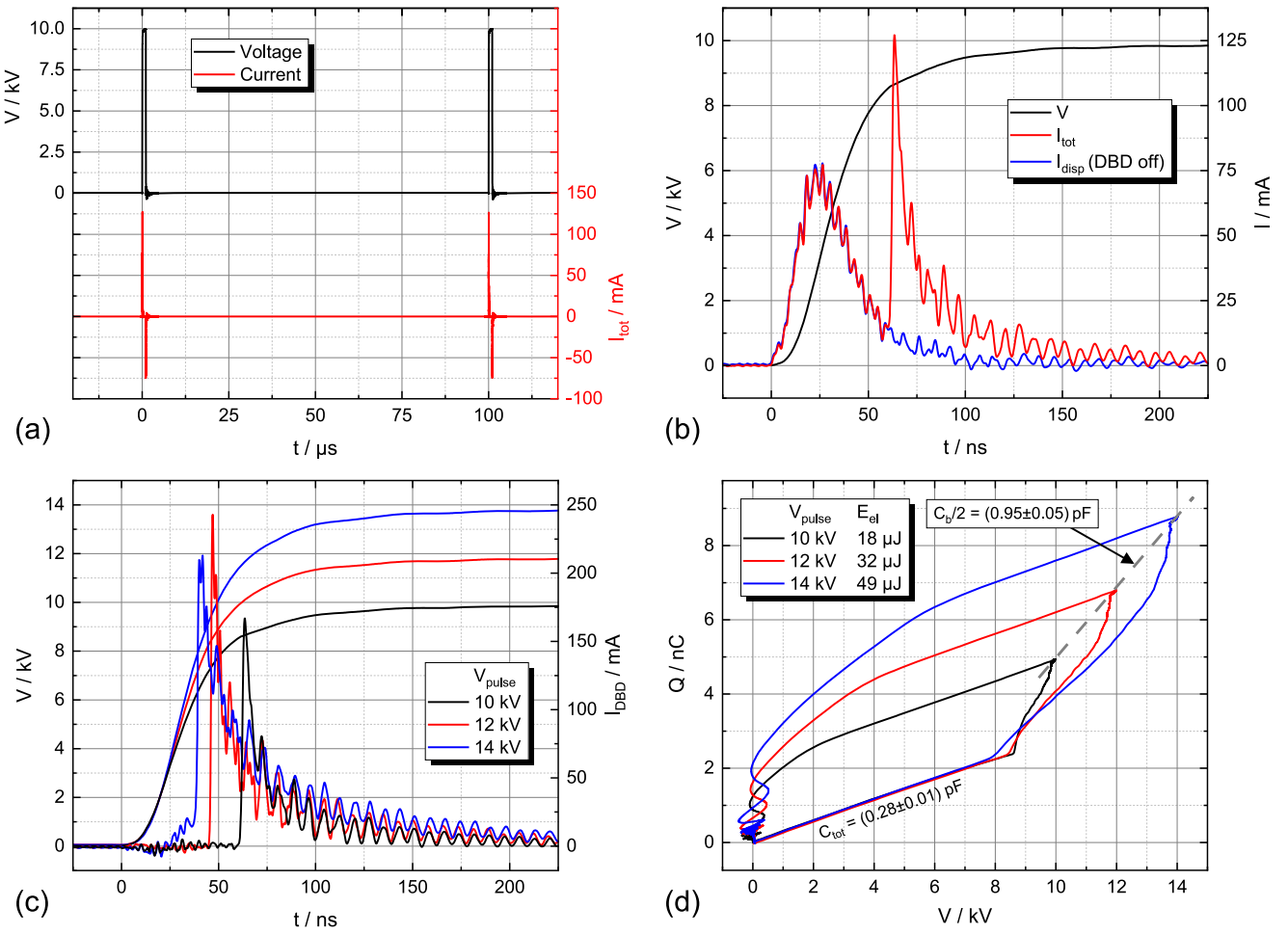

Figure 2. Electrical characteristics of pulsed DBDs with $f_{\mathrm{rep}} = 10$ kHz and $t_{\mathrm{pulse}} = 1$ μs in a 1.5 mm gap with 0.1 vol% O_2 in N_2 at $p = 1.0$ bar. All displayed results are averaged over 1000 single discharge events. (a) Overview of the applied voltage and corresponding current for $V_{\mathrm{pulse}} = 10$ kV. (b) Rising slope in detail for $V_{\mathrm{pulse}} = 10$ kV. (c) Discharge current at the rising slope for $V_{\mathrm{pulse}} = 10 \ldots 14$ kV. (d) Q–V plot providing the capacitances of the arrangement and the consumed electrical energy per HV period.

[32]. This is indicated in figure 2(d) as well and yields $C_{\mathrm{b}}/2 = (0.95 \pm 0.05)$ pF. The area enclosed by a Q–V plot equals the energy consumed per HV period. It is approximately 18 μJ for $V_{\mathrm{pulse}} = 10$ kV and increases up to approximately 49 μJ for $V_{\mathrm{pulse}} = 14$ kV.

The lower right corner of a Q–V plot corresponds to the moment of breakdown. The applied voltage required for breakdown is approximately 8.5 kV and it is generally independent of the amplitude of the applied voltage pulse. However, a lower breakdown voltage (≈7.9 kV) is observed for $V_{\mathrm{pulse}} = 14$ kV; this is a consequence of the elevated pre-ionisation level as mentioned above.

Similar measurements were performed at a pressure of 0.6 bar and in gaps with a distance of 1.0 mm and 0.5 mm, for a variety of voltage pulse amplitudes in the range from 4 to 14 kV. The aim of this voltage variation was finding specific cases with similar breakdown conditions in the gap, and thereby allowing a comparison between different gap distances and pressures. A relevant parameter regarding breakdown conditions is the reduced electric field strength E/n at the moment of breakdown t_{b}: $(E/n)_{t=t_{\mathrm{b}}} \equiv (E/n)_{\mathrm{b}}$. An estimate of the reduced electric field strength can be given based on the voltage over the gap V_{b}, the gap distance d_{gap}, and the gas density n that follows from the pressure using the ideal gas law ($n = p/(k_{\mathrm{B}}T)$, $T = 296$ K):

$$\left(\frac{E}{n}\right)_{\mathrm{b}} = \frac{V_{\mathrm{b}}}{d_{\mathrm{gap}} n} \quad \text{with} \quad V_{\mathrm{b}} = \frac{C_{\mathrm{b}}/2 - C_{\mathrm{tot}}}{C_{\mathrm{b}}/2} V(t_{\mathrm{b}}), \qquad (3)$$

where $V(t_{\mathrm{b}})$ is the applied voltage at $t = t_{\mathrm{b}}$. The required capacitances were extracted from Q–V plots for each gap distance and pressure; the obtained values are given in table 1. Although the effective capacitance of the dielectric barriers $C_{\mathrm{b}}/2$ is found to increase when increasing the gap distance or reducing the pressure, the total capacitance C_{tot} only slightly decreases with d_{gap}, as would be expected from a parallel-plate capacitor.

After analysing the results of the electrical measurements, specific voltage amplitudes were chosen for each gap distance and pressure that create similar $(E/n)_{\mathrm{b}}$ without causing appreciably elevated pre-ionisation levels. The $(E/n)_{\mathrm{b}}$ values for the selected cases are (240 ± 20) Td and (150 ± 20) Td at $p = 0.6$ bar and $p = 1.0$ bar, respectively. Therefore, a comparison of breakdown characteristics for different gap distances is possible; however, for a comparison between the two

Table 1. Total capacitance C_{tot} of the DBD arrangement and effective capacitance of the two dielectric barriers $C_b/2$ for different gap distances and pressures. The measurement error is approximately 0.01 pF for C_{tot} and 0.05 pF for $C_b/2$.

d_{gap}	C_{tot}	$C_b/2$	
		$p = 0.6$ bar	$p = 1.0$ bar
0.5 mm	0.33 pF	0.70 pF	0.51 pF
1.0 mm	0.30 pF	1.30 pF	0.60 pF
1.5 mm	0.28 pF	1.40 pF	0.95 pF

pressures the difference in the reduced electric field strength needs to be considered.

Electrical properties of the selected DBDs are presented in figure 3 for the different gap distances and pressures. Figure 3(a) displays the maximum of the discharge current I_{DBD}^{max} that was determined from the averaged current measurements. The averaging in this case leads to a slight underestimation due to the temporal jitter of the discharge occurrence; however, single current measurements were used to confirm that the deviation is relatively small compared to the uncertainty induced by the capacitances in equation (1). Values of the transferred charge per single DBD at the rising slope and the consumed electrical energy per HV period are presented in figure 3(b). Here, the transferred charge was calculated by the time integration of the discharge current, and the consumed energy was obtained from Q–V plots. The results show that the transferred charge increases almost linearly with the gap distance for the selected cases, while the increase in the consumed energy is more or less quadratic. This is in agreement with the basic physical relation between charge and energy stored on a capacitor. However, it is important to note that the dependence on the gap distance cannot be derived from figure 3, since the displayed electrical quantities (i.e. the maximum of the discharge current, transferred charge and consumed energy) are not determined by breakdown conditions only. They provide an overview of relevant physical quantities for the investigated DBDs, but a comparison between them is hardly possible and not the intention of this paper.

To investigate the spatial structure of the selected DBDs, spectrally-integrated single and accumulated iCCD images were recorded. The resulting images for the different gap distances are shown in figure 4 for $p = 1.0$ bar. All images are displayed in pseudo-colour, i.e. red indicates the highest and black the lowest intensity. The labels 'anode' and 'cathode' indicate the polarity of the potential difference established between the electrodes. In the case of a positive unipolar pulse, the powered electrode is the anode during the rising slope and the cathode during the falling slope. The value of the applied voltage is for each case given in the images as well.

The recorded DBDs consist of a constricted channel in the volume and branching discharge channels on the surface of the dielectric barriers. It needs to be emphasised that this represents the overall structure of the discharge after the streamer has crossed the gap, and not the discharge structure during the streamer breakdown phase. However, a comparison of

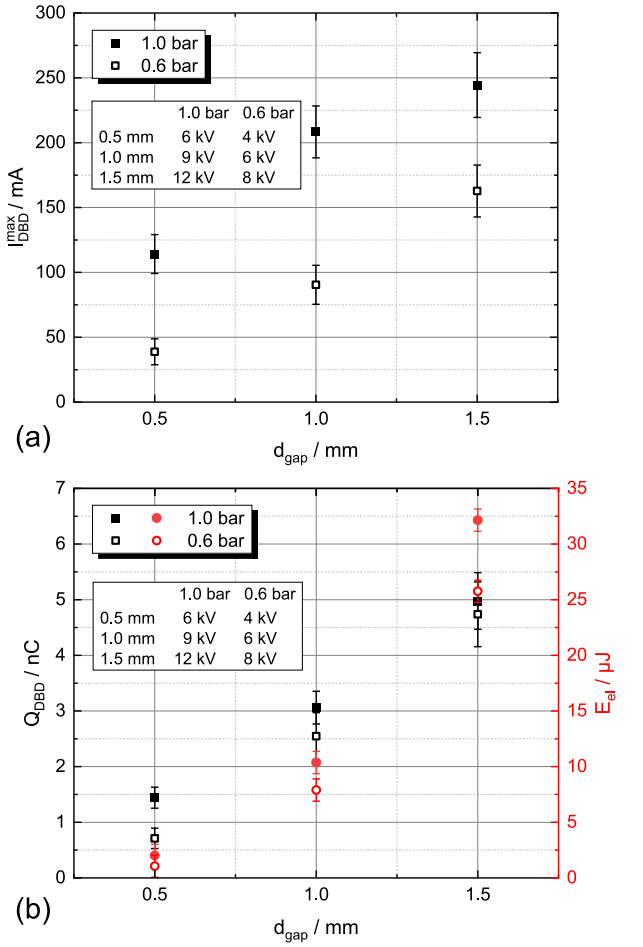

Figure 3. Electrical properties of the selected DBDs for different gap distances and pressures: (a) maximum of the discharge current, and (b) transferred charge per single DBD and consumed electrical energy per HV period. The applied voltages corresponding to the displayed cases are given in the insets.

the emission structures for different gap distances is possible despite the different applied voltages, because the emission structure hardly changes when adapting the voltage, i.e. increasing the voltage mainly affects the overall intensity but not the intensity distribution. Comparing the iCCD images in figure 4 shows that reducing the gap distance leads to an increase in the relative intensity of the surface discharge on the tip of the cathode; for discharges in a 0.5 mm gap this is even the location with the highest detected intensity. Besides a change in the intensity distribution, the extent to which the surface discharges spread over the electrodes also decreases when reducing the gap distance, and additionally a smaller number of surface discharge channels is observed. This leads to a smaller effective surface coverage that is considered to be responsible for the substantial variation in the $C_b/2$ values given in table 1.

The axial intensity distribution of the volume discharge features a structure that is similar to that of a glow discharge, with a zone of lower emission in front of the cathode (the so-called dark space analogous with glow discharges) and a zone of higher emission towards the anode. This structure is less

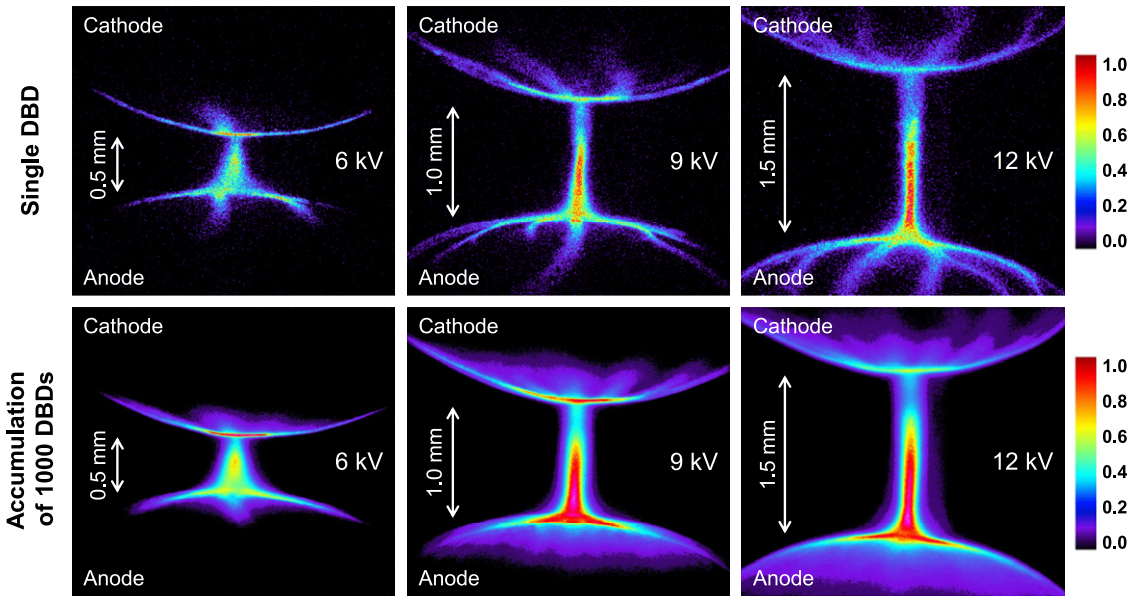

Figure 4. Comparison of iCCD images (150 ns gate width) of discharges at the rising slope for different gap distances at $p = 1.0$ bar. The amplitude of the applied voltage pulses is displayed in the images. The intensity is scaled with respect to the maximum of each image. Top: single DBD (microchannel plate (MCP) gain: 200), bottom: accumulation of 1000 DBDs (MCP gain: 0).

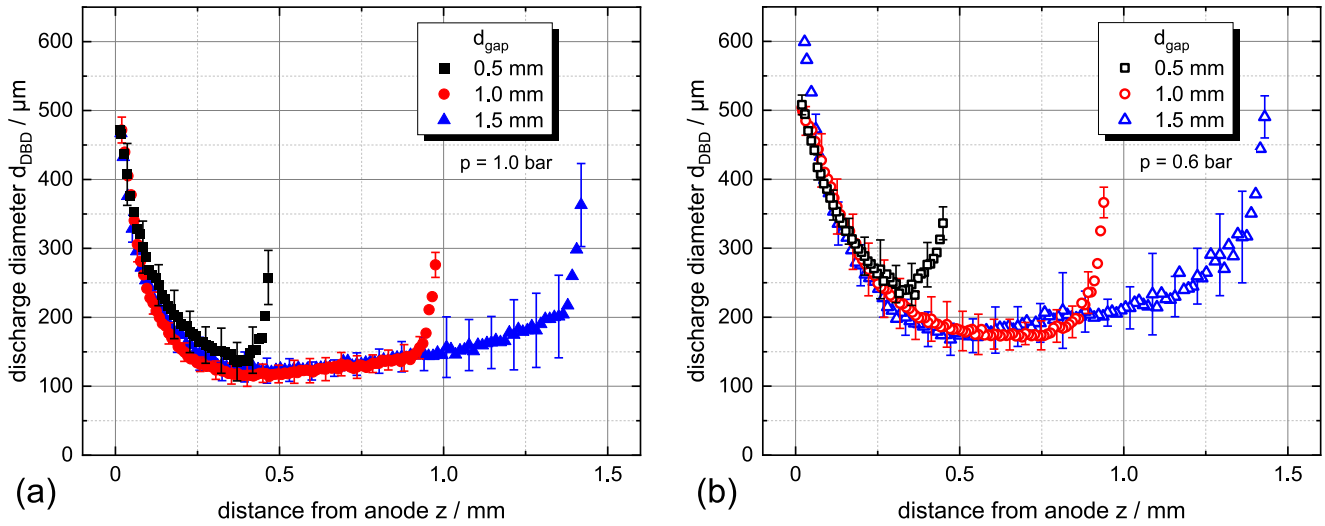

Figure 5. Comparison of the discharge diameter d_{DBD} at the rising slope for different gap distances at (a) $p = 1.0$ bar, and (b) $p = 0.6$ bar. The vertical bars do not indicate the measurement error but the spread of single data points.

pronounced in the case of a 0.5 mm gap, for which the intensity maximum is shifted towards the middle of the gap and the zone of lower emission is significantly reduced.

The diameter of the discharge channel was examined by extracting the radial emission profile throughout the entire gap from iCCD images. For this, 25 images of single DBDs were recorded, as using the accumulation of multiple DBDs can lead to an overestimation of the diameter due to a small spatial jitter of the discharge channel. The discharge diameter was in this study determined by integrating the extracted radial emission profiles and identifying the two points where the emission profiles start deviating from the noise level. This provides an accurate measure of the full width at the baseline of the emission profile; the estimated error is within 5%. The advantage of this full width in comparison with the full width at half maximum (FWHM) is that the obtained values are independent of the intensity maximum, and in addition they are hardly affected by the line-of-sight integration of the recorded emission. The resulting discharge diameters for different gap distances are shown in figures 5(a) and (b) for 1.0 bar and 0.6 bar, respectively. For all gap distances, the diameter strongly increases towards the surface of the anode. This broadening occurs within a typical distance of approximately 250 μm from the anode, independent of the proximity of the cathode, that demonstrates that varying the gap distance does not influence the structure of a filament attaching to the anode. The same effect is observed at both pressures,

although the discharge is slightly broader at a lower pressure. This change in diameter is roughly correlated with the pressure-related increase in the mean free path: $\lambda_{\mathrm{mfp}} \sim p^{-1}$. Lastly, broadening of the channel takes place in front of the cathode as well, but this cannot be accurately assessed due to the low intensity at this location.

Figure 6 shows spectrally-integrated streak images of the DBDs recorded under the same conditions as the iCCD images in figure 4. The streak images visualise the spatio-temporal development of the DBDs along the central axis of the discharge channel. The entrance slit of the streak camera had a width of 100 μm. This corresponds to an actual width of approximately 30 μm due to the optical magnification produced by the long-distance microscope, and it is therefore much smaller than the width of the discharge channel. The displayed streak images are an accumulation of several hundreds of single images that were corrected for the temporal jitter of the breakdown occurrence by means of a jitter correction procedure included in the streak camera software. The intensity is logarithmically scaled and displayed in pseudo-colour. The white lines in each image mark the position of the electrode tips. The discharge development starts with the accumulation of positive space charges in front of the anode (see e.g. [30], but not visible in figure 6) and the subsequent propagation of a cathode-directed (positive) streamer. This is followed by a transient glow-like discharge in the volume. The temporal development of the surface discharges can be seen in the streak images as well, but only directly in the centre on the electrode tips, where the streak camera slit was positioned.

Comparing the streak images for different gap distances shows that there is a slight shift of the streamer inception point away from the anode for larger gap distances. Furthermore, for larger gap distances, an additional emission structure in front of the anode is observed that emerges while the streamer is still propagating. This indicates the presence of an increasing amount of emitting species at this location even before the streamer has crossed the gap (i.e. before the actual breakdown). The structure can be observed at both pressures and it is more prominent for lower applied voltages. A similar structure was reported in [33], where it was especially evident for less steep applied voltage pulses that led to a relatively slow start of the streamer propagation.

The spatio-temporal breakdown development in the gap was analysed further with contour plots containing a collection of points within a certain intensity range. Figure 7 shows contour plots that were extracted from the streak images in figure 6. These plots trace the cathode-directed streamer during its propagation through the gap. For a better comparison, the different plots were shifted in time for the streamer to reach the cathode at the same time. From visually inspecting the contour plots, it is already obvious that the streamer propagates faster in a larger gap, since the time needed for the streamer to cross the gap is approximately the same ($\approx$1.5 ns) for all three cases.

Quantitative values for the streamer propagation velocity can be determined by a fitting of the contour plots. To get accurate results, it is necessary to take into account the limited spatial and temporal resolutions of the streak camera. This is especially of importance close to the surface of the cathode,

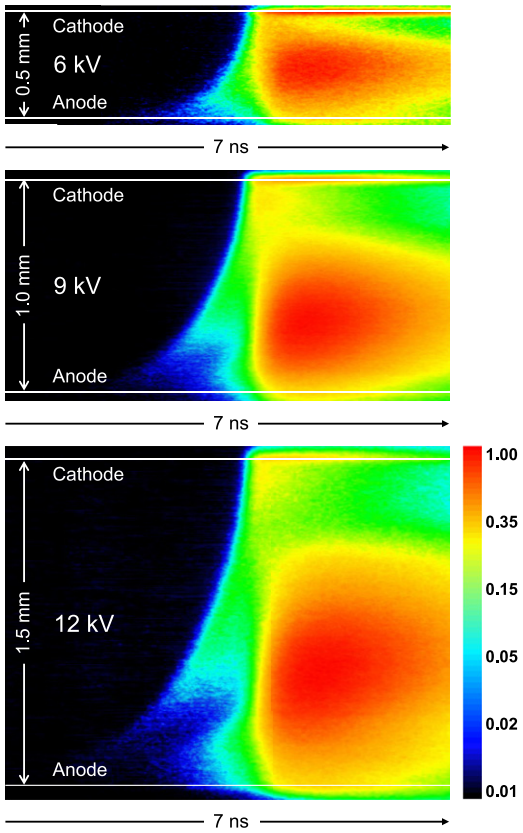

Figure 6. Comparison of streak images showing the spatio-temporal development of the DBDs at the rising slope along the central axis of the discharge channel for different gap distances at $p = 1.0$ bar. The amplitude of the applied voltage pulses is displayed in the images.

where ignoring the limited temporal resolution of 20 ps would lead to a considerable overestimation of the velocity.

The obtained streamer propagation velocities for the case of a 1.5 mm gap and a pressure of 1.0 bar are shown in figure 8(a). The streamer propagation velocity is approximately the same for $V_{\mathrm{pulse}} = 10$ and 12 kV, as expected because the breakdown conditions (i.e. the breakdown voltage and corresponding reduced electric field at the moment of breakdown) are independent of the voltage amplitude. However, for $V_{\mathrm{pulse}} = 14$ kV the streamer propagates significantly slower. This is a clear consequence of changed breakdown conditions due to the elevated pre-ionisation level in this case. When the streamer propagates slower, it generates less charge carriers per unit of time; this leads to a decrease in the discharge current maximum as already observed in figure 2(c).

The streamer propagation velocities in a 1.5 mm gap but now for a pressure of 0.6 bar are presented in figure 8(b). Here, effects due to an elevation of the pre-ionisation level are negligible. The only discernible difference between the three displayed cases is that the streamer has a slower initial velocity for $V_{\mathrm{pulse}} = 7$ kV. This is because the breakdown occurs at the relatively flat part of the applied voltage pulse in this case; however, it appears to have only a minor effect on the final velocity that is reached in front of the cathode.

The selected cases investigated in this work do not feature significant effects due to elevated pre-ionisation levels, nor do

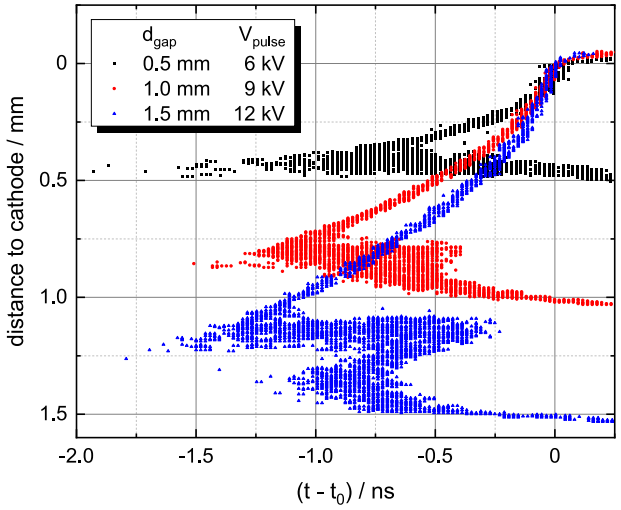

Figure 7. Contour plots extracted from streak images illustrating the propagation of the cathode-directed streamer at the rising slope for different gap distances at $p = 1.0$ bar. For a better comparison, the curves were shifted in time to reach the cathode at the same time $t = t_0$.

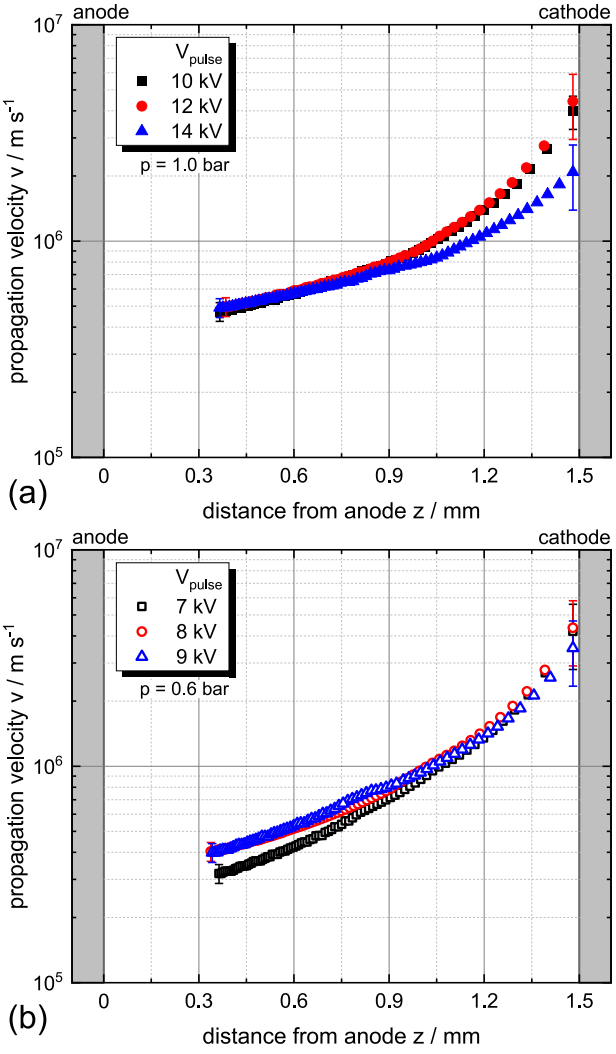

Figure 8. Propagation velocity of the cathode-directed streamer at the rising slope for different voltage pulse amplitudes in a 1.5 mm gap for (a) $p = 1.0$ bar, and (b) $p = 0.6$ bar.

they show other effects related to changes in the shape of the applied voltage pulse. In combination with the reduced electric field strength at the moment of breakdown having similar values, this allows a comparison of streamer characteristics for different gap distances. The streamer propagation velocities obtained at $p = 1.0$ bar are shown in figure 9(a). In all gaps, the streamer reaches a velocity in the order of 10^6 m s^{-1} in front of the cathode, although the initial velocity is slower for smaller gap distances. It can thus be concluded that the streamer exhibits a significantly faster acceleration in smaller gaps.

The data shown in figure 9(a) can also be plotted as a function of the normalised distance to the cathode $z^* = z/d_{\text{gap}}$. This is shown in figure 9(b), and the results for $p = 0.6$ bar are included in this figure as well. A first observation is that the results for the different pressures are rather similar, even though there is a considerable difference in the reduced electric field strength at the moment of breakdown. Additionally, for both pressures, the streamer is found to propagate faster when the gap distance is larger. Another important result is that the development of the streamer propagation velocity as a function of z^* features a similar structure independent of the real gap distance. This indicates that the proximity of the cathode has a strong impact on the propagation of the streamer.

The absolute distance between the cathode and the streamer head is expected to be especially of importance for the acceleration of the streamer, as a decrease in this distance leads to an increase in the electric field strength between the cathode and the streamer head; this leads to a higher streamer acceleration [35]. The observed differences in the acceleration for different gap distances could be explained by the changes in the inception point and initial streamer velocity, but further research including a detailed modelling of the discharge development is needed to confirm this.

Lastly, it is worth mentioning that both the streamer propagation velocity and the diameter of the streamer are connected to the electric field strength in the streamer head [36]. Previous research [37] has shown that the diameter of the streamer increases steadily during the cathode-directed propagation, correlated to an increase in the axial propagation velocity, and afterwards a rapid broadening of the discharge channel occurs when the streamer reaches the cathode. The diameter values presented in figure 5 were however extracted from iCCD images of the entire discharge, i.e. they do not represent the streamer diameter but the final diameter of the discharge channel. Therefore it remains unclear if the streamer diameter is also significantly larger in a 0.5 mm gap, or if the diameter is actually smaller and broadening of the channel is taking place just after the streamer has crossed the gap. Time-resolved iCCD images or radial streak images are needed to investigate this further, which is planned for future experiments.

Nevertheless, the results presented here already clearly demonstrate the impact of the electrode proximity on the over-

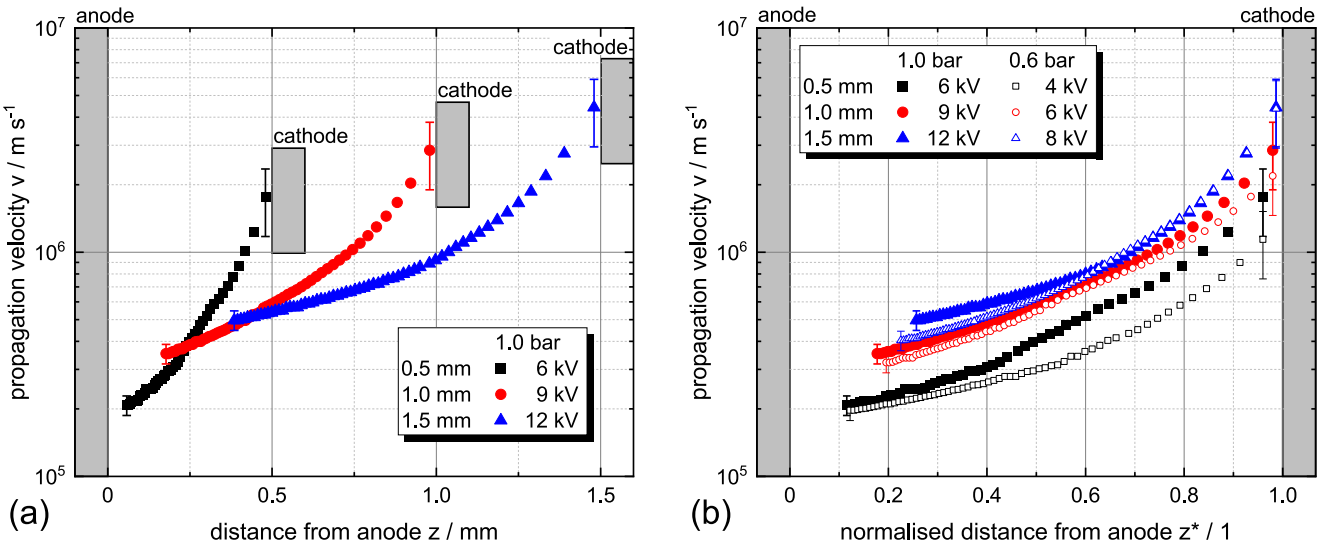

Figure 9. Comparison of the streamer propagation velocities at the rising slope for different gap distances and pressures: (a) velocity as a function of the distance from the anode z, and (b) velocity as a function of the normalised distance z^*, where $z^* = z/d_{\mathrm{gap}}$.

all discharge emission structure as well as on the axial streamer propagation velocity.

4. Summary and outlook

This study investigated the impact of the electrode proximity on the streamer breakdown and development of pulsed-driven DBDs in a single-filament discharge arrangement. This was done using a gas mixture of 0.1 vol% O_2 in N_2 at $p = 0.6$ bar and $p = 1.0$ bar. The amplitude of the applied voltage pulses was varied to create similar conditions in the gap, that allowed a comparison of breakdown characteristics for different gap distances (0.5 mm, 1.0 mm, and 1.5 mm). The reduced electric field strength at the moment of breakdown was used as the main parameter for describing breakdown conditions and it was estimated to be approximately 240 Td and 150 Td for the investigated DBDs at 0.6 bar and 1.0 bar, respectively.

The results for the streamer propagation velocity demonstrated a faster streamer propagation for larger gap distances, while in smaller gaps the streamer featured a significantly higher acceleration. This indicates that the proximity of the cathode has a strong impact on the characteristics of the streamer propagation.

Investigating the emission structure of the discharge after the streamer had crossed the gap showed that reducing the gap distance led to a shift in the location of the intensity maximum towards the middle of the gap. This was accompanied by a decrease in the extension of the surface discharges. The change in the overall emission structure was especially evident in a 0.5 mm gap, where the proximity of the electrode surfaces significantly influenced the discharge development throughout the entire gap. However, in front of the anode, the same discharge diameter and broadening thereof were found, independent of the proximity of the cathode, and it can therefore be concluded that the structure of a filament attaching to the anode is not influenced by the gap distance. Reducing the pressure resulted in broader channel diameters and lower discharge currents, but it had little effect on the investigated breakdown characteristics.

The experimental results presented in this paper are intended to be used in the future as an important input and reference for a 2D model of the discharge development for variable gap distances. This would provide further insight into the physical processes of breakdown, especially in the vicinity of the electrode surfaces in confined DBD arrangements.

Acknowledgments

This work was partly supported by the DFG project Multi-Fil (No. 408777255). Furthermore, we would like to thank U Nehmzow (glassblower, INP) and the mechanical workshop of the INP for manufacturing the discharge cell and P Mattern (INP) for discussing and programming the diameter determination routine. Additionally, we are grateful to T Hoder and P Synek from the Department of Physical Electronics at Masaryk University in Brno (CZ) for providing us with the fast current probe and to T Hoder for fruitful discussions. Finally, we would like to acknowledge A Sobota from the Department of Applied Physics at the Eindhoven University of Technology (NL) for the much appreciated cooperation and enduring support.

Data availability statement

The source data for the figures 2, 3, 5, 7, 8, and 9 are provided under https://doi.org/10.34711/inptdat.531 in the public repository INPTDAT.

ORCID iDs

J R Wubs https://orcid.org/0000-0003-2035-9099
H Höft https://orcid.org/0000-0002-9224-4103
M Kettlitz https://orcid.org/0000-0002-9216-2861
M M Becker https://orcid.org/0000-0001-9324-3236
K-D Weltmann https://orcid.org/0000-0002-4161-205X

References

[1] Schoenbach K H and Becker K 2016 *Eur. Phys. J.* D **70** 22
[2] von Woedtke T, Emmert S, Metelmann H-R, Rupf S and Weltmann K-D 2020 *Phys. Plasmas* **27** 070601
[3] Brust H, Nishime T M C, Wannicke N, Mui T S M, Horn S, Quade A and Weltmann K-D 2021 *J. Appl. Phys.* **129** 044904
[4] Kogelschatz U 2007 *Plasma Process. Polym.* **4** 678–81
[5] Ono R, Nakagawa Y and Oda T 2011 *J. Phys. D: Appl. Phys.* **44** 485201
[6] Bruggeman P and Brandenburg R 2013 *J. Phys. D: Appl. Phys.* **46** 464001
[7] Kogelschatz U 2003 *Plasma Chem. Plasma Process.* **23** 1–46
[8] Bruggeman P J, Iza F and Brandenburg R 2017 *Plasma Sources Sci. Technol.* **26** 123002
[9] Braun D, Küchler U and Pietsch G 1991 *J. Phys. D: Appl. Phys.* **24** 564–72
[10] Gibalov V I and Pietsch G 2012 *Plasma Sources Sci. Technol.* **21** 024010
[11] Greb A, Boettner H, Winter J and Schulz-von der Gathen V 2011 *Plasma Sources Sci. Technol.* **20** 055010
[12] Xiong Z and Kushner M J 2012 *Plasma Sources Sci. Technol.* **21** 034001
[13] Gibalov V I and Pietsch G J 2000 *J. Phys. D: Appl. Phys.* **33** 2618–36
[14] Hoder T, Sira M, Kozlov K V and Wagner H-E 2008 *J. Phys. D: Appl. Phys.* **41** 035212
[15] Kogelschatz U 2010 *J. Phys.: Conf. Ser.* **257** 012015
[16] Brandenburg R 2017 *Plasma Sources Sci. Technol.* **26** 053001
[17] Bogaczyk M, Nemschokmichal S, Wild R, Stollenwerk L, Brandenburg R, Meichsner J and Wagner H-E 2012 *Contrib. Plasma Phys.* **52** 847–55
[18] Tschiersch R, Bogaczyk M and Wagner H-E 2014 *J. Phys. D: Appl. Phys.* **47** 365204
[19] Akishev Y, Aponin G, Balakirev A, Grushin M, Karalnik V, Petryakov A and Trushkin N 2011 *Plasma Sources Sci. Technol.* **20** 024005
[20] Kettlitz M, van Rooij O, Höft H, Brandenburg R and Sobota A 2020 *J. Appl. Phys.* **128** 233302
[21] Yurgelenas Y V and Wagner H-E 2006 *J. Phys. D: Appl. Phys.* **39** 4031–43
[22] Pietsch G J and Gibalov V I 1998 *Pure Appl. Chem.* **70** 1169–74
[23] Bondarenko P N, Emelyanov O A and Shemet M V 2014 *Tech. Phys.* **59** 838–46
[24] Steinle G, Neundorf D, Hiller W and Pietralla M 1999 *J. Phys. D: Appl. Phys.* **32** 1350
[25] Papageorghiou L, Panousis E, Loiseau J F, Spyrou N and Held B 2009 *J. Phys. D: Appl. Phys.* **42** 105201
[26] Nemschokmichal S *et al* 2018 *Eur. Phys. J.* D **72** 89
[27] Li X, Dijcks S, Nijdam S, Sun A, Ebert U and Teunissen J 2021 *Plasma Sources Sci. Technol.* **30** 095002
[28] Kozlov K V, Wagner H-E, Brandenburg R and Michel P 2001 *J. Phys. D: Appl. Phys.* **34** 3164–76
[29] Höft H, Kettlitz M, Hoder T, Weltmann K-D and Brandenburg R 2013 *J. Phys. D: Appl. Phys.* **46** 095202
[30] Höft H, Kettlitz M, Becker M M, Hoder T, Loffhagen D, Brandenburg R and Weltmann K-D 2014 *J. Phys. D: Appl. Phys.* **47** 465206
[31] Synek P, Zemánek M, Kudrle V and Hoder T 2018 *Plasma Sources Sci. Technol.* **27** 045008
[32] Pipa A V, Hoder T, Koskulics J, Schmidt M and Brandenburg R 2012 *Rev. Sci. Instrum.* **83** 075111
[33] Höft H, Becker M M, Loffhagen D and Kettlitz M 2016 *Plasma Sources Sci. Technol.* **25** 064002
[34] Kettlitz M, Höft H, Hoder T, Reuter S, Weltmann K-D and Brandenburg R 2012 *J. Phys. D: Appl. Phys.* **45** 245201
[35] Kulikovsky A A 1997 *J. Phys. D: Appl. Phys.* **30** 1515–22
[36] Naidis G V 2009 *Phys. Rev.* E **79** 057401
[37] Höft H, Becker M M and Kettlitz M 2018 *Plasma Sources Sci. Technol.* **27** 03LT01